Investigating well potential parameters on neural spike enhancement in a stochastic-resonance pre-emphasis algorithm

Cihan Berk Güngör[1,2], Patrick P. Mercier[1], and Hakan Töreyin[2]

[1] Department of Electrical and Computer Engineering, University of California – San Diego, La Jolla, CA, USA
[2] Department of Electrical and Computer Engineering, San Diego State University, San Diego, CA, USA

E-mail: htoreyin@sdsu.edu

Received January 12th, 2021
Accepted for publication
Published xxxxxx

Abstract

Objective. Background noise experienced during extracellular neural recording limits the number of spikes that can be reliably detected, which ultimately limits the performance of next-generation neuroscientific work. In this study, we aim to utilize stochastic resonance (SR), a technique that can help identify weak signals in noisy environments, to enhance spike detectability. *Approach.* Previously, an SR-based pre-emphasis algorithm was proposed, where a particle inside a 1D potential well is exerted by a force defined by the extracellular recording, and the output is obtained as the displacement of the particle. In this study, we investigate how the well shape and damping status impact the output Signal-to-Noise Ratio (SNR). We compare the overdamped and underdamped solutions of shallow- and steep-wall monostable wells and bistable wells in terms of SNR improvement using two synthetic datasets. Then, we assess the spike detection performance when thresholding is applied on the output of the well shape-damping status configuration giving the best SNR enhancement. *Main results.* The SNR depends on the well-shape and damping-status type as well as the input noise level. The underdamped solution of the shallow-wall monostable well can yield to more than four orders of magnitude greater SNR improvement compared to other configurations for low noise intensities. Using this configuration also results in better spike detection sensitivity and positive predictivity than the state-of-the-art spike detection algorithms for a public synthetic dataset. For larger noise intensities, the overdamped solution of the steep-wall monostable well provides better spike enhancement than the others. *Significance.* The dependence of SNR improvement on the input signal noise level can be used to design a detector with multiple outputs, each more sensitive to a certain distance from the electrode. Such a detector can potentially enhance the performance of a successive spike sorting stage.

Keywords: bistable well, extracellular spike detection, monostable well, stochastic resonance

1. Stochastic Resonance for Pre-emphasis of Neural Spikes

Neural circuits in the brain represent and convey information in the form of electrical action potentials, namely neural spikes. By obtaining and analyzing these spikes, it is possible to explore the connectivity and computation in the brain.

The first step to capture and analyze neural spikes is to record neural activity by placing electrodes in extracellular tissue near the brain. An extracellular neural recording is first electronically amplified and filtered in hardware. The signal is then digitized to perform successive signal processing steps of (i) pre-emphasis to suppress the noise and enhance the spikes, (ii) detection to identify the spikes, and (iii) sorting to match the spikes with the neurons at the recording site.

Thanks to low-noise electronics design techniques and advanced signal processing methods, it is possible to suppress the interference and obtain high signal-to-noise ratio (SNR) spikes leading to improved detection and sorting performance. However, currently the number of neurons that can be monitored by a single electrode (five to ten [1, 2]) is significantly smaller than the theoretical number of ~200 that corresponds to the number of neurons inside a spherical region centered at the electrode and having a radius of ~140 μm [3]. One of the reasons for the small number of sortable spikes is that, spikes originated from distant neurons can go unnoticed due to background noise. Accordingly, these spikes are lost even at the detection step.

Potentially, the number of spikes that can be detected in an extracellular recording can be increased by improving the SNR. Accordingly, several pre-emphasis methods have been proposed over the past decade [4, 5, 6, 7, 8]. Recently in a pre-emphasis method that facilitates stochastic resonance (SR), it was shown that background noise could indeed help enhancing the spikes [9]. This counterintuitive result can be explained by considering a system consisting of a particle inside a 2D monostable well (Figure 1(a)). Here, the well can be described as a nonlinear function of the x-coordinate. A force applied on the particle along the x-axis causes the particle to move inside the well. The input to the system (i.e., a neural recording) is introduced as a force exerted on the particle and the output of the system (i.e., pre-emphasized neural recording) is the resultant displacement of the particle along the x-axis. In this system, a noise-free input, such as a noise-free neural spike, exerted onto the particle will move the particle. Compared to a noise-free signal, a noisy signal could push the particle more, and thus improving the spike amplitude at the output. Here, the intensity of the noise is important; a large noise intensity will swamp the spike, whereas a small noise intensity will not have much impact on the particle displacement. This non-linear system is essentially a non-linear filter. In [9], the output of such a non-linear filter

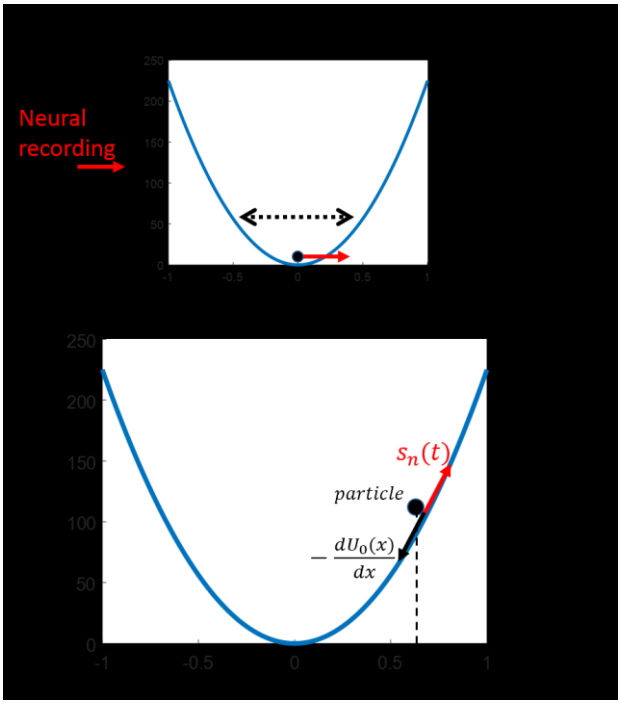

Figure 1. Stochastic resonance (SR) is facilitated to enhance neural spikes. (a) In the SR pre-emphasis approach, neural recording is applied on a particle inside a monostable well. The resultant displacement of the particle is an SNR-enhanced version of the input signal. (b) Noisy signal, $s_n(t)$, and the well slope at the particle position $-\frac{dU_0(x)}{dx}$ are two forces acting on the particle. $x(t)$ denotes the output.

is investigated when introduced with noisy extracellular recordings. By applying thresholding on the noise-enhanced recordings, detection sensitivities comparable to the state-of-the-art template-based spike detection methods were demonstrated in [9].

In this study, we investigate the pre-emphasis performances of several SR systems with different characteristics. We are motivated by, first, the detection performance of the SR-based spike enhancement. Second, the use of background noise as a facilitator of SNR improvement, which can potentially enable SNR enhancement of spikes from more distal neurons. Lastly, unlike template-based spike detection, SR-based pre-emphasis does not need *apriori* spike waveform information. Therefore, spike detection performance is not dependent on the activity level or type of neurons. Our goal is to develop insights on the parameters of an SR-based pre-emphasis system in the context of spike enhancement.

Below we describe our methods and dataset in Section 2. We present our results in Section 3 followed by a discussion in Section 4. We conclude the paper in Section 5.

2. Methods and Dataset

2.1. Stochastic-Resonance-based pre-emphasis

Stochastic resonance (SR) is a phenomenon where additive noise is used to enable detectability of a weak signal [10, 11, 12, 13]. In the context of pre-emphasis of extracellular recordings, in [9] SR has been leveraged by considering a particle in a potential well, $U_0(x)$ (Figure 1(b)). In this system, the noisy input signal, s_n, is applied as a force on the particle; and $s_n(t) = s(t) + n(t)$, where $s(t)$ is the noise-free input signal and the $n(t)$ is the noise. Another force acting on the particle is proportional to the well slope at the particle position and in the opposite direction of the slope. The output of the non-linear filter, $x(t)$, is obtained as the projection of the particle on the x-axis as the particle moves inside the well. For small-amplitude inputs, the particle tends to remain near its stable point. Larger inputs on the other hand, cause the particle to make larger swings. When using the described non-linear filter to emphasize neural spikes, $s_n(t)$ is the recorded neural signal that is inherently noisy. The neural recording, $s_n(t)$, is fed to the non-linear filter as the input. The emphasized neural recording is the output of the non-linear filter, namely $x(t)$.

In this system, depending on the signal amplitude, additive noise will affect the output differently. For low-amplitude inputs such as spike-free regions of an extracellular recording, random variations in the signal due to noise will not persistently exert a force on the particle to push it away from the stable point, thereby limiting the output amplitude. In other words, the existence of a stable point will facilitate noise suppression. On the other hand, when the particle moves towards a wall due to a large-amplitude signal such as a spike, additive noise, $n(t)$, may increase the input, $s_n(t)$, assisting the particle to move away from the stable point and thus enhancing the output amplitude. Importantly, there is an optimum noise intensity: Small noise intensities would not have much impact on the particle movement, whereas large noise intensities would cause the particle make large but random movements in the well.

The expression describing the input-output relationship of the non-linear filter is governed by the generalized Langevin equation as [14]:

$$\frac{d^2x(t)}{dt^2} + \gamma \frac{dx(t)}{dt} = -\frac{dU_0(x)}{dx} + s_n(t), \qquad (1)$$

where $x(t)$ is the output of the filter and γ is damping factor.

Based on equation (1), one of the parameters that may affect the output is the well shape, $U_0(x)$. Specifically, the number of stable points and slope of the walls should affect the force exerted on the particle by the wall. For instance, as the steepness of the wall increases, the force $-\frac{dU_0(x)}{dx}$ would increase, and thus making it more difficult for the particle to rise along the wall. The number of stable points of the well is also expected to affect the output signal amplitude. Considering a particle in a bistable well, a noisy-spike input can be sufficiently large to move the particle across the unstable equilibrium point and thus carrying it from one stable point to the other. In that case, the x-position (i.e., the output) of the particle, will be affected by the distance between the stable points.

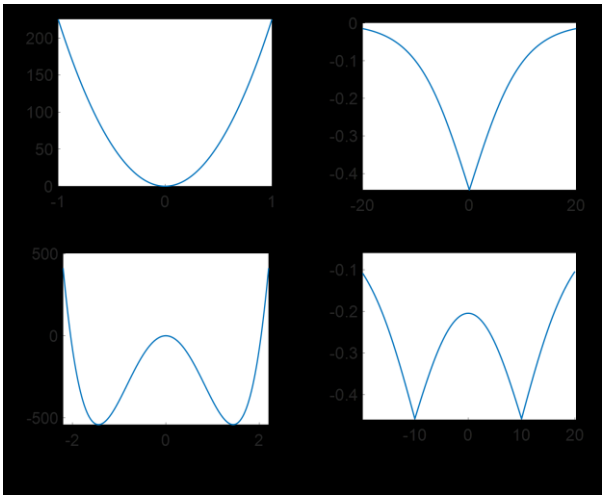

Figure 2. The well shapes investigated. (a) Shallow-slope monostable well potential. (b) Steep-slope monostable well potential. (c) Shallow-slope bistable well potential. (d) Steep-slope bistable well potential.

In addition to the well shape, damping status is also expected to impact the output. On the left-hand side of equation (1), if γ is large, which corresponds to an overdamped case, the inertia term (the second-order time derivative) is negligible compared to the damping term (the first-order time derivative term). An underdamped case corresponds to a small γ, where both inertia and damping terms are considered. The previous implementation of the SR-based spike pre-emphasis method in [9] is an overdamped system. However, inertia can potentially be used to enhance the output SNR: The existing acceleration of a particle due to the large perturbation in the input signal (i.e., noisy spike) could be favorable to achieve larger displacement and thus output.

It should be noted that, in the scenario where inertia is included, low perturbations in the input (i.e., noise-only portions of a neural recording) would also cause larger swings and therefore impairing the noise suppression performance. To potentially address the issue, the damping of the system could be dynamically controlled depending on the amplitude of the input signal. As such, while the particle would take advantage of its acceleration during large amplitude portions of the input, large damping during small amplitude portions would limit its movement.

2.2. Well-shape and damping combinations

Based on the discussion on well shape and damping status above, we investigate the responses of different well-shape and damping combinations (Figure 2).

Shallow-slope monostable (ShM) well (Figure 2(a)): The first monostable well we consider is the one investigated in the SR-based neural spike improvement in [9]. Another motivation for investigating a monostable well is related to potentially achieving high sorting performance on the pre-emphasized spikes. The movement of a particle inside a monostable well is expected to be continuous, which would limit potential disruptions in the output spike waveform shapes. This well and its derivative for the dimension x are described as:

$$U_{ShM}(x) = ax^2/2 + bx^4/4. \quad a, b > 0 \tag{2}$$

$$U'_{ShM}(x) = ax + bx^3. \quad a, b > 0 \tag{3}$$

It should be noted that, it is possible to define a shallow-slope monostable well using alternative expressions. The expression in equation (2) is selected for its convenience in describing the bistable version of the shallow-slope well by simply using negative values for a. To compare with the previous implementation in [9], we investigate this well first for the overdamped case (ShM-OD). Second, we investigate the well for an underdamped response (ShM-UD). Following the damping coefficient discussion in Section 2.1, we adjust the damping dynamically depending on the input such that it is reduced when the input is large. Specifically, for $s_n < \frac{s_{n,pp}}{d_{th}}$ we set the $\gamma = 120$. For $s_n \geq \frac{s_{n,pp}}{d_{th}}$, we set the $\gamma = 0.12$. Here $s_{n,pp}$ is the peak-to-peak value of the entire recording and $d_{th} = 10$ is the damping threshold.

Steep-slope monostable (StM) well (Figure 2(b)): Following the discussion on equation (1) regarding the potential effect of wall slope on particle displacement, we also investigate the response in a monostable well having steeper slopes around the stable point, namely Wood-Saxon (WS) well [15].

To compare with the shallow-slope overdamped results in [9], we consider an over damped case for the WS well (StM-OD). The WS well potential and its derivative are given as:

$$U_{StM}(x) = \frac{V}{1+\exp((|x|-R)/a)}. \quad V > 0, R > 0, a > 0 \tag{4}$$

$$U'_{StM}(x) = -\frac{V}{a} sgn(x) exp\left(\frac{|x|-R}{a}\right)\left(1 + exp\left(\frac{|x|-R}{a}\right)\right)^{-2}. \quad V > 0, R > 0, a > 0 \tag{5}$$

In (5), V, R, and a respectively control the depth, width, and wall-slope of the well potential. The SNR improvement StM wall is expected to work as follows: A steep slope around the stable point would hamper the particle movement during small-amplitude noise-only portions of the neural recording, which would translate into strong noise suppression. On the other hand, a noisy neural spike would allow the particle to move up along the wall. A decreasing slope along the wall would translate into greater particle displacement, and thus enhanced spike at the output.

Shallow-slope bistable (ShB) well (Figure 2(c)): In addition to the monostable wells, we investigate the response to a shallow-slope bistable well, the classic well used to describe the SR for periodic signals [16]. A shallow-slope bistable well potential and its derivative are given as:

$$U_{ShB}(x) = ax^2/2 + bx^4/4. \quad a < 0, b > 0 \tag{6}$$

$$U'_{ShB}(x) = ax + bx^3. \quad a < 0\ b > 0 \tag{7}$$

For ShB well to enhance the neural spikes, it is anticipated that a noisy spike would be able to switch the particle from one stable point to the other. On the other hand, a noise-only section would move the particle only around a stable point.

First, we investigate an overdamped response of the shallow-slope bistable well (ShB-OD). Second, to ease switching between the stable points during spike events and impede the transition during noise-only sections, we implement a dynamic damping (ShB-UD) similar to the implementation explained in ShM-UD.

Steep-slope bistable (StB) well (Figure 2(d)): We also investigate the response in a bistable well having both steep slopes around the stable points.

To compare with the overdamped response of the shallow-slope bistable well, we consider an overdamped case for the steep-slope bistable well (StB-OD). The steep-slope bistable well potential is obtained as the sum of two StM wells described by equation (4). The two StM wells are separated by a variable. The StB well and its derivative are given as:

$$U_{StB}(x) = U_{StM}(x - sep) + U_{StM}(x + sep). \quad V > 0, R > 0, a > 0, sep > 0 \tag{8}$$

$$U'_{StB}(x) = U'_{StM}(x - sep) + U'_{StM}(x + sep). \quad V > 0, R > 0, a > 0, sep > 0 \tag{9}$$

In (9), V, R, a, sep respectively control the depth, width, wall-slope, and stable point separation of the steep-slope bistable well potential. It is anticipated that, a StB would facilitate the noise suppression mechanism of steep wall and spike enhancement mechanism of a bistable well.

2.3. Numerical solution of the SR system

The solution to equation (1) can be approximated by an iterative numerical method, namely the fourth-order Runge-Kutta (RK) method [14, 17]:

$$x[n+1] = x[n] + (p_1 + 2p_2 + 2p_3 + p_4)h/6, \tag{10}$$

$$y[n+1] = y[n] + (k_1 + 2k_2 + 2k_3 + k_4)h/6, \tag{11}$$

where $x[n]$ is the nth sample of $x(t)$ and $y[n]$ is the nth sample of $\frac{dx(t)}{dt}$. In equations (10) and (11), k_1 through k_4 and p_1 through p_4 are given as:

$$\begin{aligned} k_1 &= \left[-U_0'(x[n]) - \gamma p_1 + s_n[n]\right] \\ k_2 &= \left[-U_0'\left(x[n] + \frac{p_1 h}{2}\right) - \gamma p_2 + s_n[n]\right] \\ k_3 &= \left[-U_0'\left(x[n] + \frac{p_2 h}{2}\right) - \gamma p_3 + s_n[n+1]\right] \\ k_4 &= \left[-U_0'(x[n] + p_3 h) - \gamma p_4 + s_n[n+1]\right]. \end{aligned} \tag{12}$$

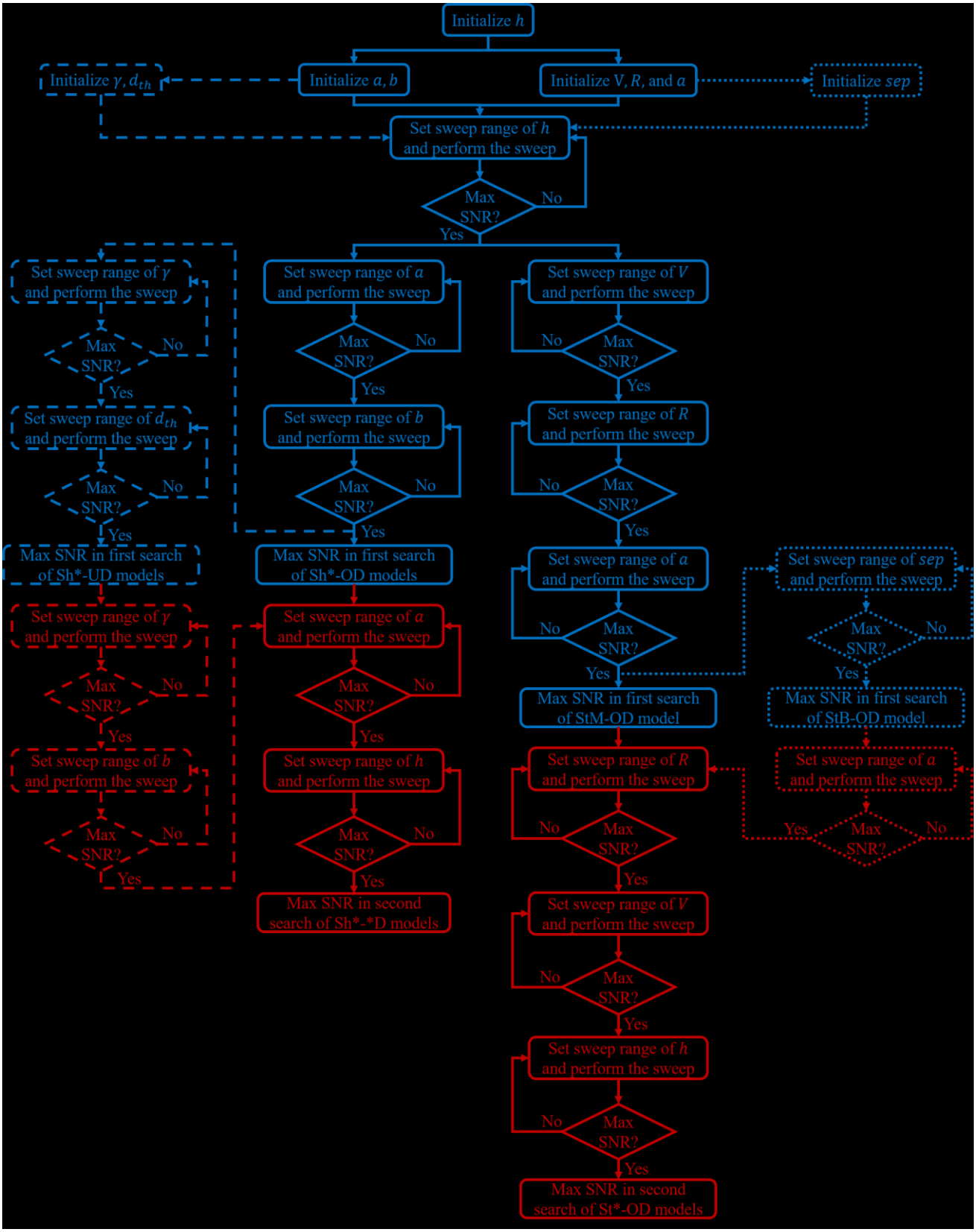

Figure 3. Flow diagram of the parameter optimization for each well-solver configurations. First and second parametric search of the parameters are given with blue and red, respectively.

Table 1. The parameters of well-solver configurations

Model type	Solver parameter	Well parameters	Damping parameters
ShM-OD	h	a, b	-
ShM-UD	h	a, b	γ, d_{th}
ShB-OD	h	a, b	-
ShB-UD	h	a, b	γ, d_{th}
StM-OD	h	V, R, a	-
StB-OD	h	V, R, a, sep	-

$$\begin{aligned} p_1 &= y[n] \\ p_2 &= y[n] + \frac{k_1 h}{2} \\ p_3 &= y[n] + \frac{k_2 h}{2} \\ p_4 &= y[n] + k_3 h. \end{aligned} \quad (13)$$

In (12) and (13), h is the interval size of the RK approximation; and $s_n[n]$ and $s_n[n+1]$ are respectively the nth and n+1st samples of $s_n(t)$. For the overdamped solution cases, only the equations (10) and (12) are used after the modifications of p_i in equation (10) are changed to k_i, where $i = 1,2,3$ and $\gamma = 0$ in equation (12).

To optimize performance, we perform a parametric search for the well and solver parameters (i.e., $a, b, V, R, sep, h, \gamma, d_{th}$) towards maximizing the output SNR defined as:

$$SNR = 20log\left(\frac{App\ of\ spike}{Standard\ deviation\ of\ a\ noise\ segment}\right), \quad (14)$$

where A_{pp} is the average peak-to-peak amplitude of 20 arbitrarily selected spikes in the employed dataset. We calculate the standard deviation of noise from 20 noise-only segments with a total duration of 2 s.

2.4. Well-solver parameter selection

The selection of the parameters is performed through a series of parametric search maximizing ΔSNR. The parameters of different well-solver configurations are summarized in Table 1. The parameter optimization flow is carried out over three steps consisting of (i) initialization, (ii) parametric search of the parameters with an order of solver/well/damping parameters, and (iii) parametric search of the parameters with the reverse order of damping/well/solver parameters.

At the initialization step, the parameter initialization is performed following the values in the literature as follows: h = 5*10^{-5} (for all models) [18], a = 1000 (for ShM) or -1000 (for ShB) [19], b = 1000 (for ShM and ShB) [19], γ = 1 (for ShM and ShB) [20, 21], d_{th}= 2 (for ShM and ShB), a = 0.4 (for StM, StB), V = 3 (for StM and StB), R = 0.5 (for StM and StB) [22], sep = 1 (for StB). The orders of parameter optimization in the two steps following the initialization step are presented in Figure 3. Optimization of each parameter involves first identifying the search limits, then sweeping

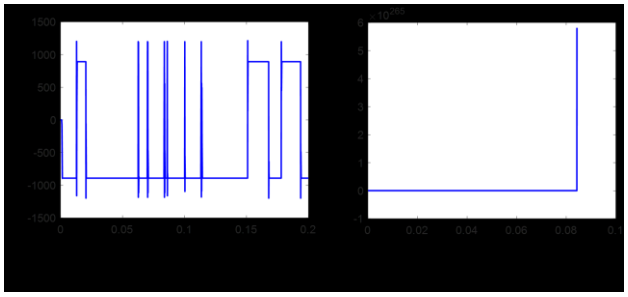

Figure 4. The output when h parameter is (a) inside and (b) outside the search range. Note the diverging output in (b).

within the limits, and lastly selecting the value providing the highest ΔSNR. Search ranges of all parameters are determined as the ranges that the output does not diverge. To illustrate the divergence of the output, example outputs when the h value is inside and outside the search range are shown in Figure 4.

2.5. Thresholding for spike detection

Following the SR-based pre-emphasis implemented on each of the aforementioned well-shape and damping status configurations, we use thresholding to determine the spikes. When comparing different configuration models, threshold levels are swept to obtain receiver operating characteristic (ROC) curve and area under curve (AUC) values. For a deeper investigation on the detection performance of the ShM-UD for the recordings in the 1st dataset, threshold levels giving the minimum false negative (*FN*) and false positive (*FP*) values are selected. Sensitivity (*Se*) is defined as the ratio between number of spikes correctly detected, namely true positive (*TP*), and the total number of spikes in the recording. Positive predictivity (*Pp*) is defined as the ratio between true positives and the total number of detected spikes:

$$Se\ (\%) = \frac{TP}{TP+FN} * 100 \quad (15)$$

$$Pp\ (\%) = \frac{TP}{TP+FP} * 100 \quad (16)$$

We used *FN*, *FP*, *Se*, and *Pp* as metrics of performance assessment and comparison.

2.6. Datasets

We use two datasets to evaluate and compare the different well-shape and damping-status configurations used in the SR-based pre-emphasis method. The first dataset is a publicly available synthetic extracellular dataset [4]. In the literature, this dataset is widely used as a benchmark to evaluate spike detection algorithms [23, 24, 25, 26, 27]. The dataset consists of 16 recordings grouped as Easy1, Easy2, Difficult1, and Difficult2. Recordings, each 60 s long and sampled at a rate of 24 kHz, use actual *in-vivo* spike waveforms from three different neurons. Each neuron has an average firing rate of 20 Hz. Background noise in the recordings is modeled after the activity of far neurons by superimposing arbitrarily selected spikes from the database at random times and amplitudes. The

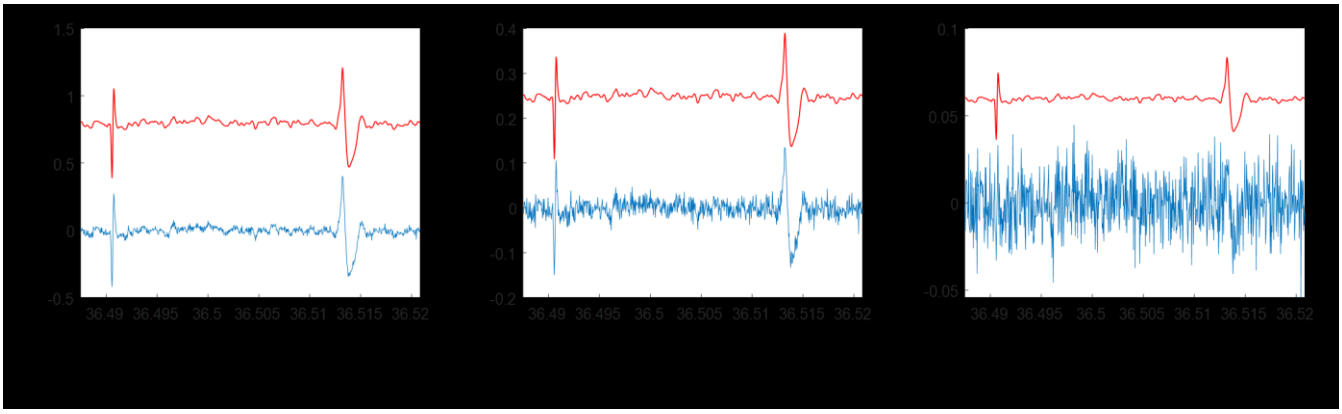

Figure 6. Sample portions of $s(t)$ (red) and $s_n(t)$ (blue) for (a) $r = 0$ µm, (b) $r = 55$ µm, and (c) $r = 105$ µm. The waveforms in (b) and (c) are obtained by adding a noise density of 0.0001 to scaled versions of the waveform in (a) based on the equation (17).

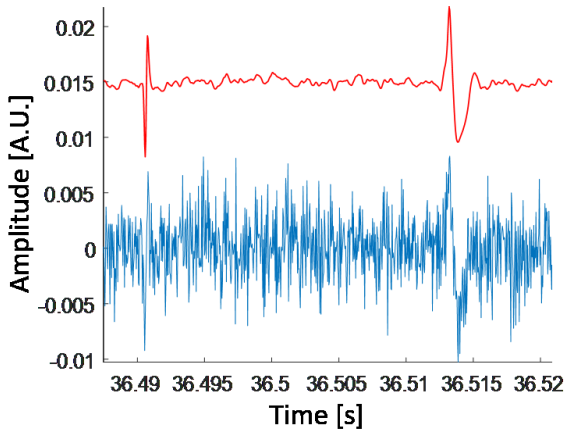

Figure 5. Sample portion of the signal (red) and signal + noise (blue) for the maximum distance of 140 µm. Spike and noise amplitudes are equal to each other in a complete recording.

noise levels in the recording name (e.g., *_noise**005***, *_noise**02***) corresponds to the noise standard deviation calculated as the ratio of spike amplitude to the noise standard deviation. We use the largest SNR recording in this dataset, *Easy1_noise005* (SNR=15.25 dB), to compare the different configurations of well potential and damping conditions. Then, we use the entire dataset for a comparison against the state-of-the-art spike-detection methods. True spike locations provided with the dataset are used to assess the detection performance as described in Section 2.4.

The second dataset consists of 20 recordings obtained by scaling the *Easy1_noise005* recording of the first dataset and adding gaussian white noise (GWN) at different intensities such that each recording represents a hypothetical condition, where only neurons at a specific distance from the electrode, r, are firing. We use this dataset to assess the performance of the algorithms in detecting the spikes at a particular distance. We consider the spikes in the original recording, *Easy1_noise005*, as being generated by neurons adjacent to the electrode (i.e., $r = 0$). To estimate the spike amplitudes corresponding to $r > 0$, we use the following exponential model presented in [28]:

$$A_{dist} = A * e^{-r/r_0}, \quad (17)$$

where A is the spike amplitude of neurons adjacent to the electrode (i.e., $r = 0$), A_{dist} is the scaled amplitude of the spike based on the distance, and r_0 is the distance that the amplitude drops to $1/e$ of A. In this study, the value of r_0 is selected as $r_0 = 28\,\mu m$, which is the experimentally-measured value in different neural recording environments [28]. It should be noted that although the spike amplitude in an extracellular recording decays with r; the background noise at the recording site, remains constant for all spikes [29]. To identify the background noise level, we use the following measurement-based observation in [3] and [28]: Spikes of neurons that are ~140 µm away from the electrode are smaller than the noise floor and thus cannot be detected. Therefore, we set the background noise peak-to-peak value to be equal to the average spike amplitude, A_{dist}, originating from neurons with $r = 140\ \mu m$. We calculate the average A_{dist} using arbitrarily-selected 20 spikes. In Figure 5, a portion of the recording corresponding to $r = 140\ \mu m$ is shown. We initially create synthetic recordings for four r values, $r = [0, 25, 55, 105]\ \mu m$. Here $r = [0, 25]\ \mu m$ fall inside the region ($r < 50\ \mu m$), where spike amplitudes of neurons are sufficiently large (i.e., >60 μV) and thus can be detected [3]. The remaining 16 recordings are created by adding GWN with standard deviations calculated as $\sqrt{2 * D}$, where $D = 0.0001, 0.001, 0.01, 0.1$. For $r = [25, 55, 105]\ \mu m$, sample signals for noise density of 0.0001 are shown in Figure 6.

3. Results

We conduct the analysis over two steps. First, we compare configurations of well-shape and damping-status in terms of their SNR improvements. Second, we compare the spike-detection performance of the ShM-U with the state-of-the-art spike detection algorithms.

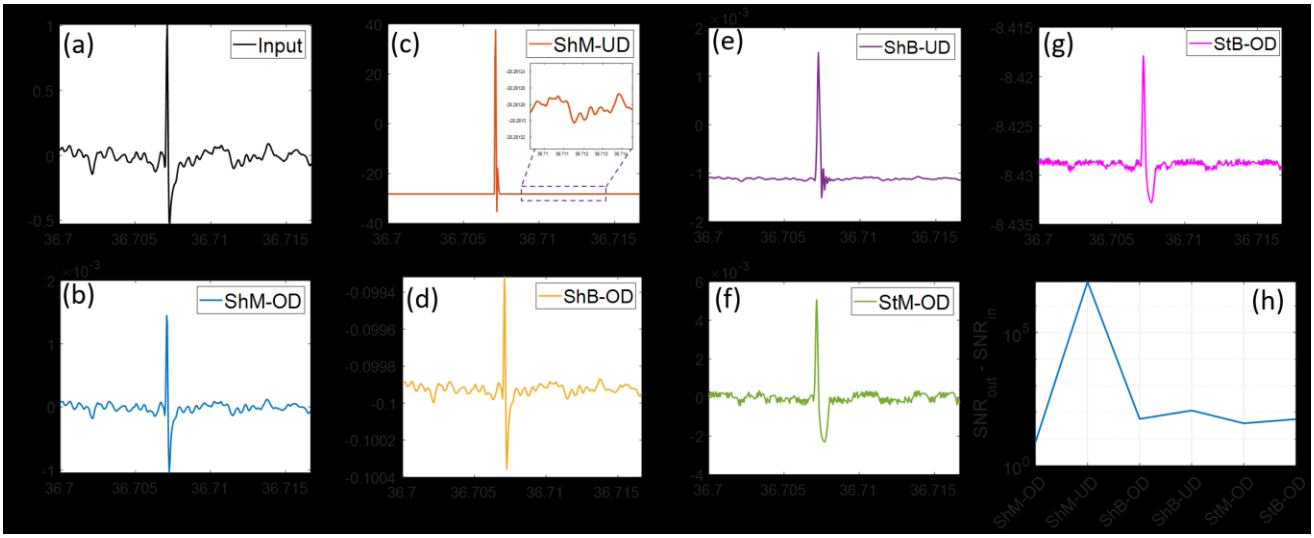

Figure 7. A spike portion of the input signal when enhanced with the SR-based pre-emphasis algorithm using the tested configurations of spike-shape and damping status. (a) The input spike. (b) ShM-OD output (c) ShM-UD output. (d) ShB-OD output. (e) ShB-UD output. (f) StM-OD output. (g) StB-OD output. (h) Average $\Delta SNR = SNR_{out} - SNR_{in}$ values calculated using 20 spikes for all configurations.

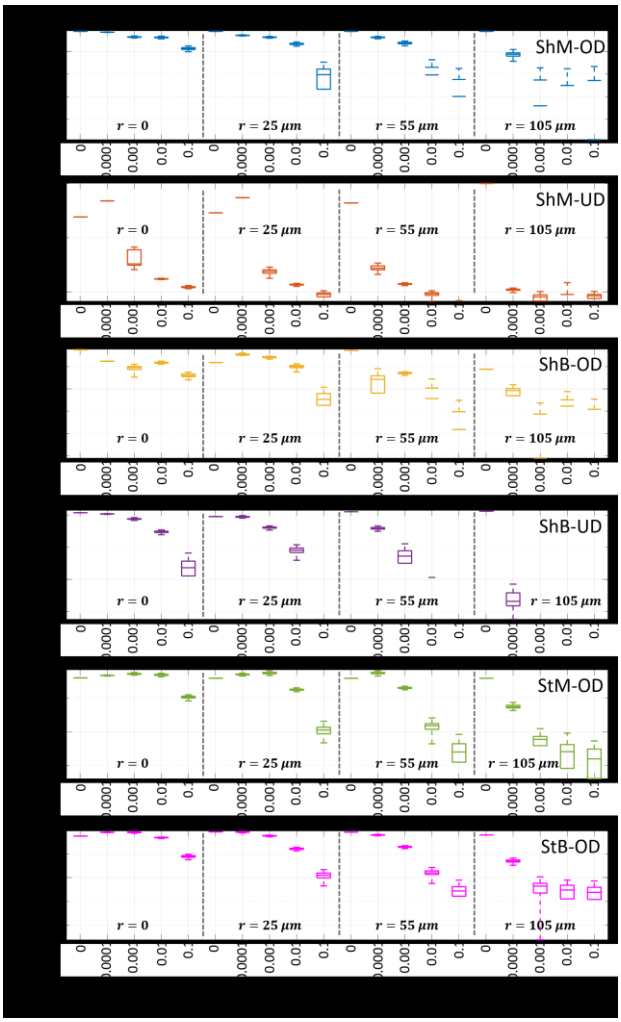

Figure 8. Statistics of SNR improvements of each well-solver configurations with 100 realizations of GWN.

We conduct the comparison using (1) the *Easy1_noise005* of the 1st dataset (Figure 7) without any noise addition and (2) the 2nd dataset (Figures 8 and 9). For each input having an SNR of SNR_{in}, the configurations of well-shape and damping condition are optimized individually based on the procedure explained in Section 2.4, to obtain the largest SNR at the output signal, SNR_{out}. For each combination, the SNR improvement is calculated as $\Delta SNR = SNR_{out} - SNR_{in}$, where SNR_{in} and SNR_{out} are calculated using 20 arbitrarily-selected spikes in the input and output signals, respectively.

For a sample spike in *Easy1_noise005* shown in Figure 7(a), the output waveforms of the different combinations are presented in Figure 7(b)-(g). ΔSNR for all configurations for *Easy1_noise005* is presented in Figure 7(h). The SNR improvement analysis on the entire 2nd dataset, where GWN is added on the *Easy1_noise005* at different intensities, is performed on 100 recordings per noise intensity: Each of the 100 recordings is obtained by adding a unique GWN dataset. Accordingly, for each noise intensity, 100 different ΔSNR is calculated. The statistics of SNR improvement are presented as box plots in Figure 8. To compare the different model configurations, the Friedman non-parametric statistical test is applied on the ΔSNR values in Figure 8. This comparison is followed by the Wilcoxon signed rank post-hoc testing for pairwise comparison of the configurations. Lastly, false-discovery-rate-corrected p-values, namely q-values, are obtained following [30]. For statistical significance analysis, q-values are used. For each of the 20 recordings of the 2nd dataset, 15 pairwise statistical significance comparisons are made between the six configuration models. Among the 300 pairwise comparisons, all configurations were statistically significantly different ($q < 0.001$) except the 32 configuration pairs presented in Table 2.

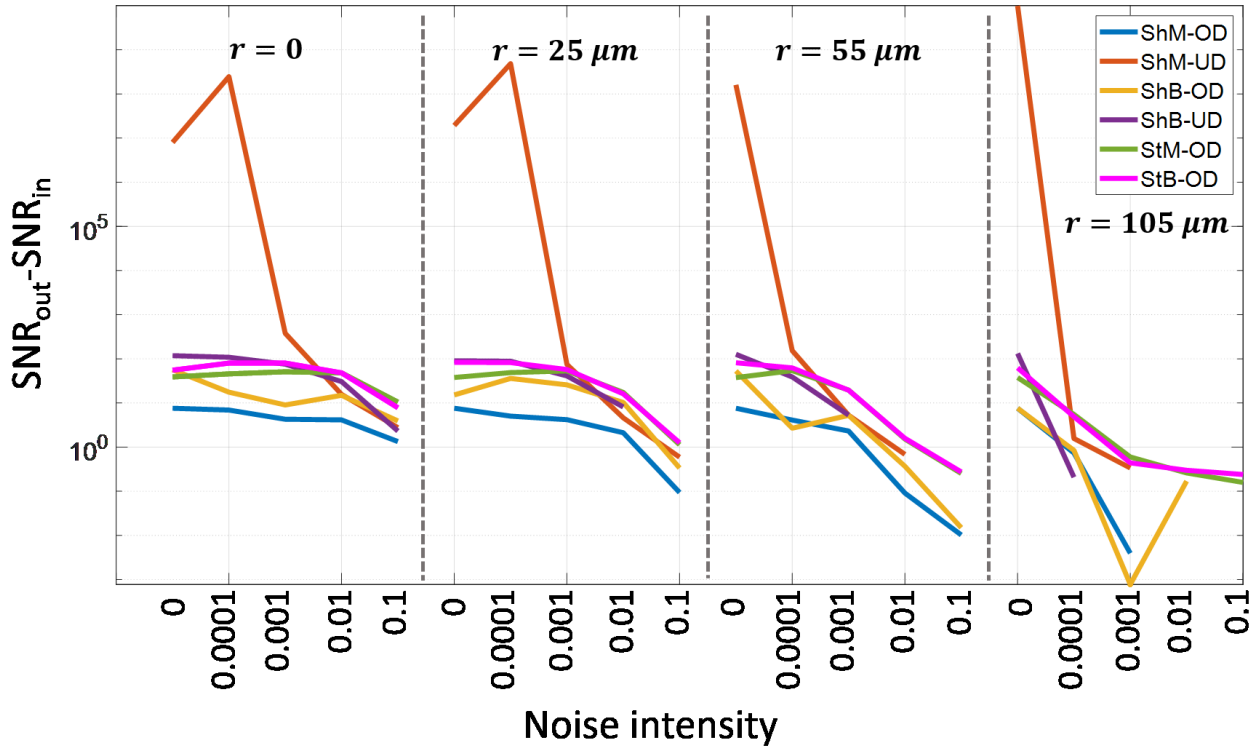

Figure 9. The median ΔSNR obtained from the outputs of each configuration.

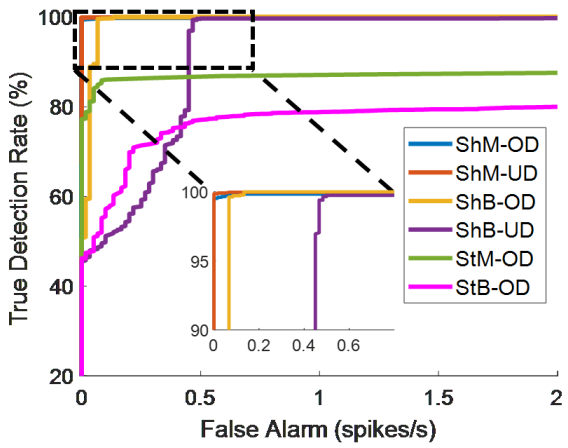

Figure 10. ROC curves for all well-solver configurations. The inset is the magnified portion of the ROC curves to show difference between ShM-OD, ShM-UD, and ShB-OD.

The median ΔSNR from each configuration model for all recordings is presented in Figure 9. The results in Figures 7, 8, and 9 reveal that, the ShM-OD combination, which is the well shape-damping status configuration presented previously in [9], yields to the smallest ΔSNR for *Easy1_noise005* and smallest median ΔSNR for the 2nd dataset.

A comparison on the model configurations is performed also in regards of the true detection vs. false alarm rates, as presented in Figure 10. True detection rate (TDR) is defined

Table 2. The configuration pairs that are not statistically significantly different

r + Noise Density	Configuration pair	q value
0 μm + 0.001	ShB-UD, StB-OD	0.1174
0 μm + 0.01	ShM-UD, ShB-OD	0.1244
0 μm + 0.01	StM-OD, StB-OD	0.1327
0 μm + 0.1	ShM-UD, ShB-UD	0.0046
25 μm + 0.001	ShM-UD, StM-OD	0.0082
25 μm + 0.001	ShM-UD, StB-OD	0.0824
25 μm + 0.001	StM-OD, StB-OD	0.0183
25 μm + 0.01	ShB-OD, ShB-UD	0.0036
25 μm + 0.01	StM-OD, StB-OD	0.0028
25 μm + 0.1	ShM-UD, ShB-OD	0.0012
25 μm + 0.1	StM-OD, StB-OD	0.0032
55 μm + 0.0001	ShM-OD, ShB-OD	0.0089
55 μm + 0.001	ShM-UD, ShB-OD	0.268
55 μm + 0.001	ShM-UD, ShB-UD	0.268
55 μm + 0.001	ShB-OD, ShB-UD	0.268
55 μm + 0.001	StM-OD, StB-OD	0.268
55 μm + 0.01	ShM-UD, ShB-OD	0.0731
55 μm + 0.01	StM-OD, StB-OD	0.1332
55 μm + 0.1	ShM-OD, ShB-OD	0.1339
55 μm + 0.1	StM-OD, StB-OD	0.1339
105 μm + 0.0001	ShM-OD, ShB-OD	0.1318
105 μm + 0.0001	StM-OD, StB-OD	0.0796
105 μm + 0.001	ShM-OD, ShB-OD	0.1388
105 μm + 0.001	ShM-UD, StB-OD	0.0776
105 μm + 0.001	StM-OD, StB-OD	0.0871
105 μm + 0.01	ShM-OD, ShM-UD	0.0478
105 μm + 0.01	ShB-OD, StM-OD	0.1654
105 μm + 0.01	ShB-OD, StB-OD	0.1108
105 μm + 0.01	StM-OD, StB-OD	0.2349
105 μm + 0.1	ShM-OD, ShB-OD	0.1121
105 μm + 0.1	ShM-UD, StB-OD	0.0149
105 μm + 0.1	StM-OD, StB-OD	0.0335

as the ratio between TPs and the total number of spikes in a recording. False alarm rate (FAR) is defined as the number of FPs per second.

$$TPR\ (\%) = \frac{TP}{TP+FN} * 100 \quad (18)$$

$$FAR = \frac{FP}{recording\ time\ (s)}. \quad (19)$$

Here, the input signal used is *Easy1_noise005*. The threshold levels are swept between 0.1σ and 10σ where σ is the standard deviation of the noise segment. The models using shallow-wall monostable well achieve better AUC than the others. Specifically, AUC of ShM-UD and ShM-OD are 99.87% and 99.86%, respectively. The third best AUC is obtained from ShB-OD configuration with a value of 97.4%. The AUC of StM-OD, ShB-UD, and StB-OD are respectively 84.4%, 80.64%, and 65.9%.

Based on SNR improvement and AUC obtained from the true detection vs. false alarm rates for the recording *Easy1_noise005*, the ShM-UD outperforms better than the other configurations. Accordingly, the spike detection performance of ShM-UD is assessed using all recordings in the first dataset. The results along with a comparison with the state-of-the-art spike detector algorithms are presented in Table 3. The results are discussed in the following section.

4. Discussion

The comparison of the two monostable wells for an overdamped solution using *Easy1_noise005* (Figure 7), shows that $\Delta SNR_{StM-OD} = 16\ dB$, and $\Delta SNR_{ShM-OD} = 8\ dB$.

For all recordings in the 2nd dataset, the overdamped solution of the StM well consistently performs better than the ShM well (Figures 8 and 9). This difference between the two configurations is statistically significant for all recordings ($q < 0.001$). The difference between the median ΔSNR of the two wells varies between 11.8 dB ($r = 105\ \mu m$ with noise intensity 0.001) and 6.94 dB ($r = 55\ \mu m$ with noise intensity 0). The significant improvement in the signal enhancement can be explained by how the wall slope changes with $|x|$. In the shallow-slope and the steep-slope monostable wells, the slope respectively increases and decreases with $|x|$ (Figure 2(c)). Compared to the ShM well, in the StM well; for a noise-only input, the particle is exposed to a large $|-\frac{dU_0(x)}{dx}|$, limiting its movement to within small proximity of the stable point. On the other hand, when the particle is exerted an input sufficiently-large to make it move away from the stable point (e.g., noisy spike), the decreasing slope of the wall will facilitate the particle movement, thereby allowing it to reach a larger $|x|$. The opposite is true for the interaction of the particle with the ShM well. The small slope around the stable point results in a worse noise suppression than the StM case for noise-only input segments; whereas, the increasing slope with $|x|$ limits the farthest point the particle can reach when the input is a noisy spike.

The overdamped well responses of the *Easy1_noise005* (Figure 7) also show that the shallow-wall bistable well spike enhancement ($\Delta SNR = 17.5\ dB$) is greater than the shallow-wall monostable well ($\Delta SNR = 8\ dB$). The ShB-OD performs better than ShM-OD, also for the recordings in the second dataset (Figure 9), except two recordings; $r = 55\ \mu m$, noise intensity = 0.0001 and $r = 105\ \mu m$, noise intensity = 0.001. Notably, for recordings, where median ΔSNR obtained from ShB-OD is more than 3 dB greater than ShM-OD (i.e., all noise intensities when $r = 0\ \mu m$ and $r = 25\ \mu m$; and noise intensities of 0.001, 0.01, 0.1 when $r = 55\ \mu m$), the comparison between ShB-OD and ShM-OD is statistically meaningful ($q < 0.001$). On the other hand, for the other

Table 3. Detection performance of the ShM-UD SR system and the other state-of-the-art using the synthetic extracellular dataset in [4]

		# of Spikes	*This Work* ShM-UD SR-system				[24] Wave_clus, BOTM, SIC		[25] PBOTM		[26] Two side thresholding		[4] BPF		[27] MRTDE	
			#FN	*#FP*	*Se (%)*	*Pp (%)*	*# FN + FP*	*Se (%)*	*# FN + FP*	*Se (%)*	*#FN*	*#FP*	*#FN*	*# FP*	*Se (%)*	*Pp (%)*
Easy1	0.05	3514	0	0	100	100	11	99.7	68	98.1	17	9	17	711	93.75	100
	0.1	3522	0	0	100	100	4	99.9	58	98.4	26	32	2	57	93.28	100
	0.15	3477	0	0	100	100	8	99.8	63	98.2	61	114	145	14	95.50	100
	0.2	3474	1	2	99.97	99.94	9	99.7	84	97.6	170	212	714	10	95.54	99.07
Easy2	0.05	3410	0	0	100	100	2	99.9	58	98.3	34	5	0	0	92.86	100
	0.1	3520	0	0	100	100	6	99.8	47	98.7	27	2	0	2	93.60	100
	0.15	3411	0	0	100	100	4	99.9	52	98.5	55	12	10	1	93.33	98.00
	0.2	3526	2	2	99.94	99.94	6	99.8	78	97.8	259	157	376	5	90.60	99.07
Diff1	0.05	3383	0	0	100	100	2	99.9	58	98.3	30	0	1	63	93.07	100
	0.1	3448	0	0	100	100	18	99.5	57	98.3	34	4	0	10	96.08	100
	0.15	3472	1	0	99.97	100	9	99.7	61	98.2	68	21	8	6	95.83	100
	0.2	3414	4	5	99.88	99.85	20	99.4	92	97.3	175	169	184	2	96.15	100
Diff2	0.05	3364	0	0	100	100	8	99.8	53	98.4	31	2	0	1	94.44	100
	0.1	3462	0	0	100	100	5	99.9	38	98.9	21	2	0	5	95.50	100
	0.15	3440	0	0	100	100	8	99.8	61	98.2	60	33	3	4	92.38	100
	0.2	3493	6	8	99.83	99.77	36	99.0	91	97.4	302	162	262	2	91.00	92.86

BOTM = Bayes optimal template matching, SIC = Subtractive interference cancellation, PBOTM = Preselection Bayes optimal template matching, BPF = Band-pass filtering, MRTDE = Multiresolution time-dependent entropy

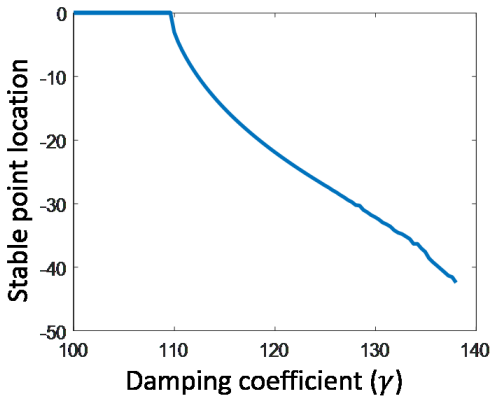

Figure 11. The stable point location change with increasing γ for an input with a negative dc level of -0.01.

recordings (including the two recordings where ShB-OD is worse than ShM-OD), the differences between the configurations are not statistically significant (q values ranging between 0.0089 and 0.1388).

The SNR improvement of the shallow-wall bistable well can be explained by the existence of a second stable point. If the input is sufficiently large to move the particle across the unstable equilibrium point between the two stable points, the output is rewarded by the well gravitating the particle towards the other stable point. During a noise-only input portion, the particle will remain trapped in one of the stable points.

It should be noted that a shallow-wall bistable well does not necessarily perform better than a monostable well. In fact, for most recordings (15 out of 20) the ShB-OD performs worse than the StM-OD. Notably, for the two recordings, where the bistable well yields greater median ΔSNR (i.e., $r = [0, 55]\ \mu m$ and noise intensity is 0), the ΔSNR differences are less than 1.6 dB. The differences between ShB-OD and StM-OD are statistically significant ($q < 0.001$) for all recordings except for the recording $r = 105\ \mu m$ with a noise intensity of 0.01 ($q = 0.1654$).

These results from the bistable and monostable wells could potentially point to the collective importance of number of stable points and the wall steepness in the output *SNR*. In fact, a steep-wall bistable well outperforms the shallow-wall bistable well in all recordings for overdamped solutions. The difference between the median ΔSNR from the StB-OD and ShB-OD varies between 1.85 dB and 13.6 dB. The two configurations are statistically significantly different ($q < 0.001$) for all recordings except for the $r = 105\ \mu m$ and noise intensity of 0.01 ($q = 0.1108$). The StB-OD and StM-OD SNR improvements are very similar for all recordings. The difference between the median ΔSNR for these configurations is limited to 2.4 dB. Notably, for $r = [0, 25, 55]\ \mu m$ with noise intensities of 0 and 0.0001; the median ΔSNR of StB-OD is greater than StM-OD. Remarkably, for those recordings, the two configurations are statistically significantly different ($q < 0.001$). For the recordings, where median ΔSNR from the two configurations differ only by less than 0.4 dB, the two configurations are not statistically significantly different ($0.0028 < q < 0.268$).

Another observation made on the Figures 7, 8, and 9 is that for the ShB well, the underdamped solutions perform better than the overdamped solutions for (i) $r = 0\ \mu m$ all noise intensities except 0.1; (ii) $r = 25\ \mu m$ noise intensities 0.001 or smaller; (iii) $r = 55\ \mu m$ noise intensities 0.0001 or smaller; and (iv) $r = 105\ \mu m$ noise intensity of 0. For those recordings, the underdamped and overdamped solutions of the ShB well are statistically significantly different ($q < 0.001$). Only for the two of the remaining four recordings, where both models produce positive median ΔSNR, the two models are statistically significantly different. Notably, while the overdamped solution of the shallow-wall bistable well performs worse than the StM-OD in 15 of the recordings, underdamped solution of the shallow-wall bistable well yields to either greater or comparable median ΔSNR compared to the StM-OD with median ΔSNR difference between the two configurations being limited to 1.6 dB. The configurations of StM-OD and ShB-UD are statistically significantly different ($q < 0.001$).

The difference between the underdamped vs. overdamped performances of the ShM well is more significant than the ShB well: For all recordings, where both ShM-OD and ShM-UD produce positive median ΔSNR, the ShM-UD performs better than the ShM-OD. The difference between the median ΔSNR from these two configurations can be as large as 91.1 dB. These configurations are statistically significantly different for all recordings ($q < 0.001$).

For *Easy1_noise005*, the configuration that produces significantly better ΔSNR than the others is the underdamped solution of the shallow wall monostable well. The differences between the ShM-UD and the others based on the performance on *Easy1_noise005* are statistically significant ($q < 0.001$). In fact, ShM-UD can lead to up to five orders of magnitude better ΔSNR than the others. We believe, this performance can be attributed to the monostable system transitioning to a bistable system via adaptive adjustment of the damping coefficient: Notably, in a shallow-wall monostable well with a constant γ value, the position of the stable point is dependent to γ and the dc level of the input. If γ is small, a spike will move the particle away from the stable point of *0*, but as soon as the spike ceases, the particle will move back to the stable point. However, a larger γ combined with a non-zero dc level may shift the stability point, which is illustrated in Figure 11. For an input with a negative dc level of -0.01, the stable point of the ShM moves in the negative *x* direction with increasing γ. Changing γ as the particle moves can result in two stable points. Small γ during a spike will allow the particle to move to an *x*-position away from its starting point. Increasing γ when the input becomes small at the end of a spike will

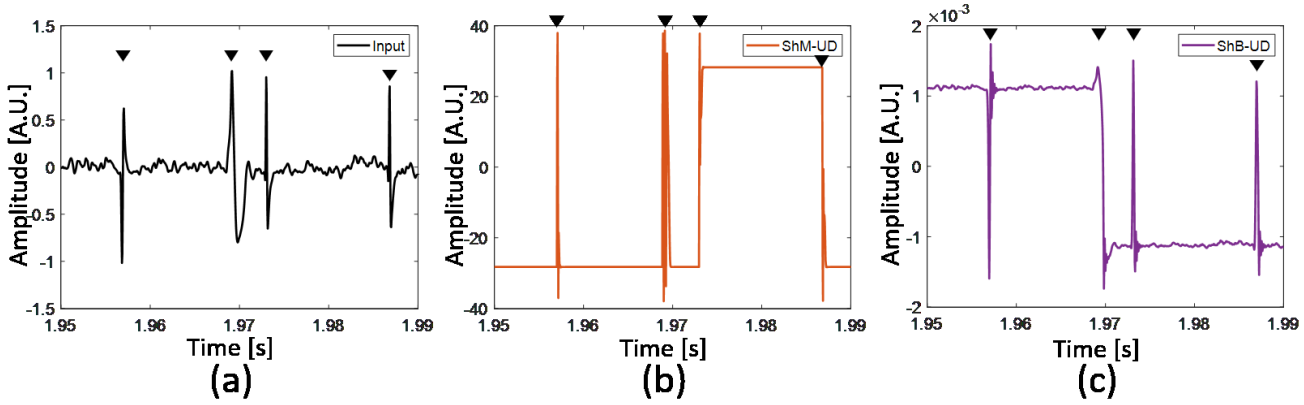

Figure 12. Bistable behavior of ShM-UD due to the dynamic adjustment of the damping coefficient. (a) A portion of input signal and the corresponding outputs from the (b) ShM-UD and (c) ShB-UD. Spike locations are marked with black triangles.

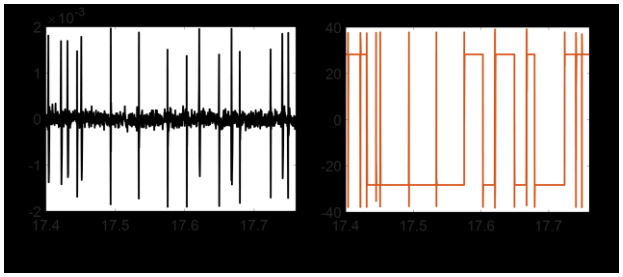

Figure 13. An output portion obtained using the ShM-UD model (a) without and (b) with adaptive damping coefficient adjustment.

Table 4. Estimated r values for eight recordings in the second dataset.

r + Noise Intensity	$r_{calculated}$ (μm)	*Best ΔSNR*
25 μm + 0	25	ShM-UD
55 μm + 0	55	ShM-UD
25 μm + 0.0001	72	ShM-UD
25 μm + 0.001	105	ShM-UD
25 μm + 0.01	135	StM-OD
105 μm + 0.0001	152	StM-OD
55 μm + 0.01	170	StM-OD
55 μm + 0.1	250	StM-OD

prevent the particle from moving back to its original point and the particle will sway around its new x location. This acquired bistable behavior of the ShM-UD is visible in the output: Similar to the ShB-UD output, ShM-UD output also switches between two stable points as shown in Figure 12. Supporting our hypothesis that adaptive damping control of the ShM leads to the bistable behavior, an ShM-UD model without adaptive damping coefficient adjustment has only one stable point (Figure 13).

Performance comparison of different models in terms of how accurately the true spikes are being detected while limiting the false detections reveals that the shallow-monostable well achieves the greatest AUC. Despite the greater ΔSNR achieved from the underdamped solution of the shallow-slope bistable well, ~17% greater AUC is obtained from the overdamped solution of the well. This can be explained by the higher rate of stable point switching caused by background noise. The high amplitude noise segments result in spike-like portions at the output, which result in high number of false alarms. The overdamped solution of the steep-slope monostable well demonstrates steep increase in true detection rate for false alarm rates smaller than 0.05. On the other hand, the true detection rate is limited to 83% for even the false alarm rate increases beyond 24, thereby limiting the AUC at 84.4%. A similar behavior is observed for the bistable version of the overdamped steep-wall. The true detection rate reaches 78% at when the false alarm rate is 0.8 but remains there between 0.6 and 4, which results in an AUC of 65.9%. The fact that true detection rates of steep-wall wells remain relatively constant for a wide range of false alarm rate can be associated with the dependence of the response of steep-slope wall well to the spike width: The output amplitude is high for wide spikes and low for narrow spikes. As the threshold is lowered between the high and low amplitude spike outputs, the false alarm rate increases without changing the true detection rate.

The average sensitivity and positive predictivity values obtained by thresholding the recordings in the first dataset after pre-emphasizing using the ShM-UD configuration are both 99.97% (Table 3). For this dataset, the SR-based ShM-UD pre-emphasis algorithm achieves better detection performance than the state-of-the-art algorithms.

The ΔSNR results in Figures 8 and 9 can also be analyzed in the context of how spike enhancement varies with the distance from the electrode, r. Increasing r, like increasing noise intensity, reduces SNR. Using equation (17), we calculated the r values corresponding to eight datasets in the second dataset (Table 4). Waveforms corresponding to the r values and illustration of a hypothetical recording site are presented in Figure 14. Based on the results, for $r \leq 105\ \mu m$; the ShM-UD configuration offers significantly better ($>78\ dB$) SNR improvement than the others. For $r \geq 135\ \mu m$, the StM-OD configuration yields greater ΔSNR than the others. However, the degree of superiority decreases with

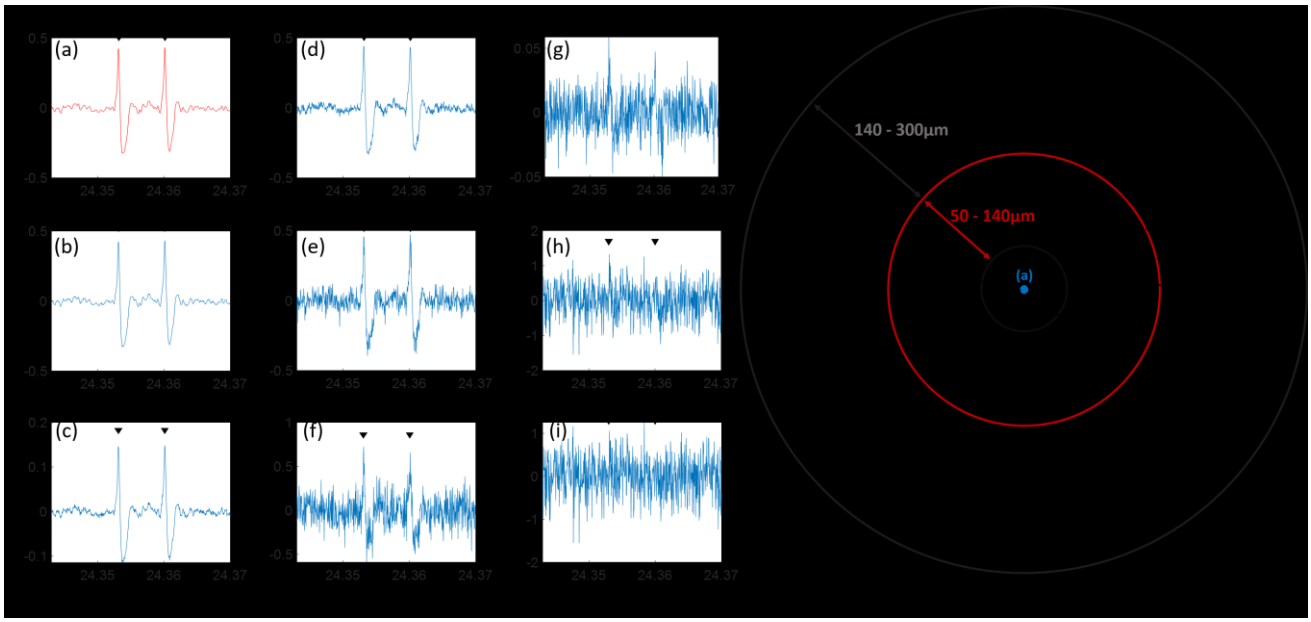

Figure 14. Sample portions of the input signal with noisy signals for each distance shown on 2D representation of spherical volume around an electrode. Spike locations are marked with black triangles for each plot (a)-(i). (a) Sample portion of input signal. (b) Sample portion of the noisy signal for a point at 25 µm. (c) Sample portion of the noisy signal for a point at 55 µm. (d) Sample portion of the noisy signal for a point at 72 µm. (e) Sample portion of the noisy signal for a point at 105 µm. (f) Sample portion of the noisy signal for a point at 135 µm. (g) Sample portion of the noisy signal for a point at 152 µm. (h) Sample portion of the noisy signal for a point at 170 µm. (i) Sample portion of the noisy signal for a point at 250 µm. (j) 2D representation of spherical volume around an electrode.

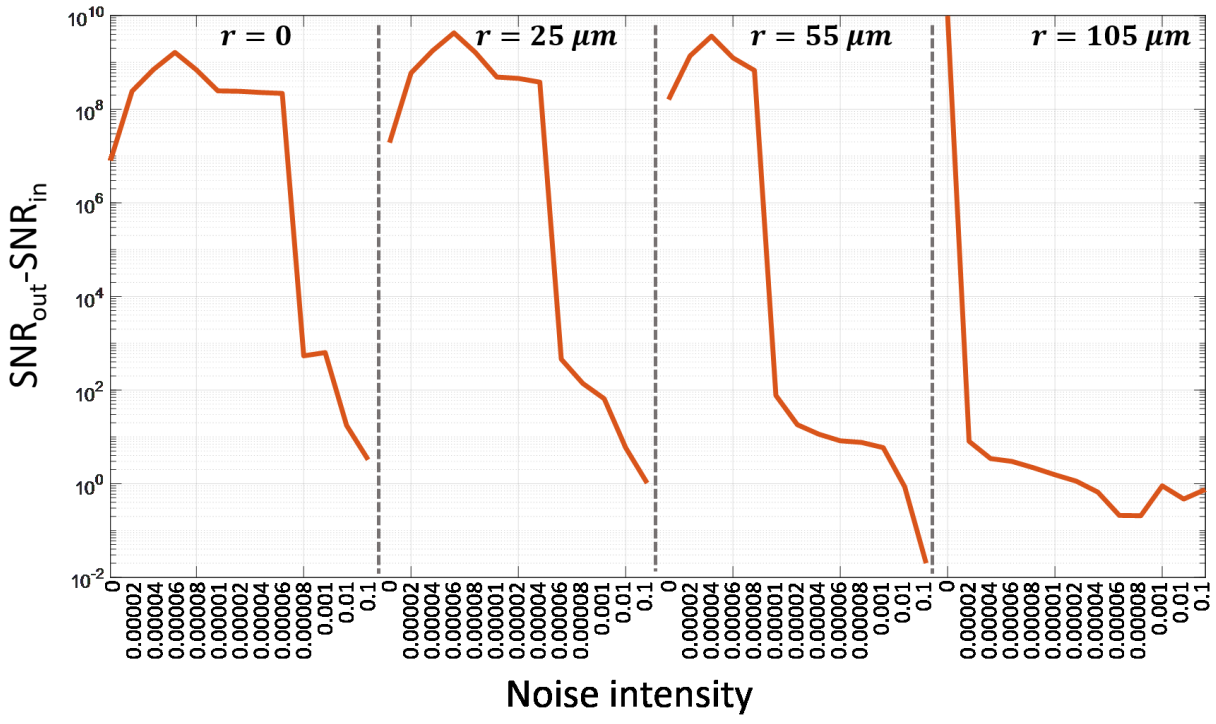

Figure 15. The $\Delta SNR = SNR_{out} - SNR_{in}$ for ShM-UD configuration with smaller steps in noise density.

r is increased. For $r = 135\ \mu m$, the difference between the SNR_{out} of StM-OD and ShB-UD, the second-best performing configuration, is ~9 dB. However, the difference reduces to ~4 dB for $r = 152\ \mu m$ and <1.5dB for $r = 170\ \mu m$ and $r = 250\ \mu m$. The configuration type using which the best ΔSNR values are obtained for each r are also summarized in Table 4.

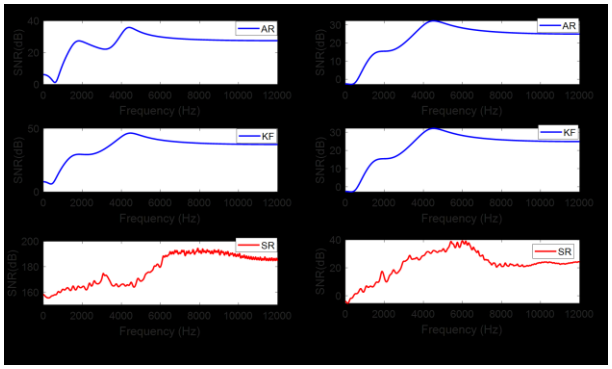

Figure 16. The *SNR* vs frequency plots of AR, KF, and ShM-UD configuration (labeled as SR) for a low noise (*Easy1_noise005*) and a high noise (*Easy1_noise02*) recording. (a) SNR comparison of AR, KF, and SR for the low noise recording. (b) SNR comparison of AR, KF, and SR for the high noise recording.

The abrupt drop in ΔSNR performance of the ShM-UD with r and superior ΔSNR performance of StM-OD for spikes originated from distant neurons may be facilitated to implement a spike detector having parallel SR-based pre-emphasis algorithms implemented using different well-shape and damping status configuration. In addition to increasing the number of spikes detected, such an amplitude-sensitive detector can group spikes with similar amplitudes and therefore potentially improve the performance of a successive spike sorting stage.

Notably, the ΔSNR variation for $r = [0, 25]\ \mu m$ in Figures 8 and 9 demonstrate an increase of ΔSNR for a non-zero noise intensity (0.0001). To investigate an optimum noise intensity level that maximizes the ΔSNR, the ShM-UD is assessed for when the noise intensity is increased with smaller increments within the noise range where the ΔSNR increase is observed (Figure 15). The results show that for $r = [0, 25, 55]\ \mu m$, ΔSNR follows the characteristic bell curve shape of SNR peaking at a noise intensity of 0.0006 for $r = [0, 25]\ \mu m$ and 0.0004 for $r = 55\ \mu m$. The bell curve shape is not observed for $r = 105\ \mu m$. These results reflect that, in this study, it is the intensity of the noise that facilitates the SR in the proposed non-linear SR pre-emphasis technique. The SR can enhance the spikes significantly better for when the noise intensity is at an optimum level. In the dataset modeling recordings closer to the electrode (i.e., $r = [0, 25, 55]\ \mu m$) the original dataset background noise is below the optimum noise intensity level. Therefore, adding more noise can further improve the SNR. Furthermore, as expected, the intensity of noise that needs to be added on the original recording to maximize the SNR is less for $r = 55\ \mu m$ than $r = [0, 25]\ \mu m$. On the other hand, for the dataset modeling the recording farthest from the electrode, the noise level of the original recording is higher than the optimum noise intensity, and thus any additional noise only decreases the SNR.

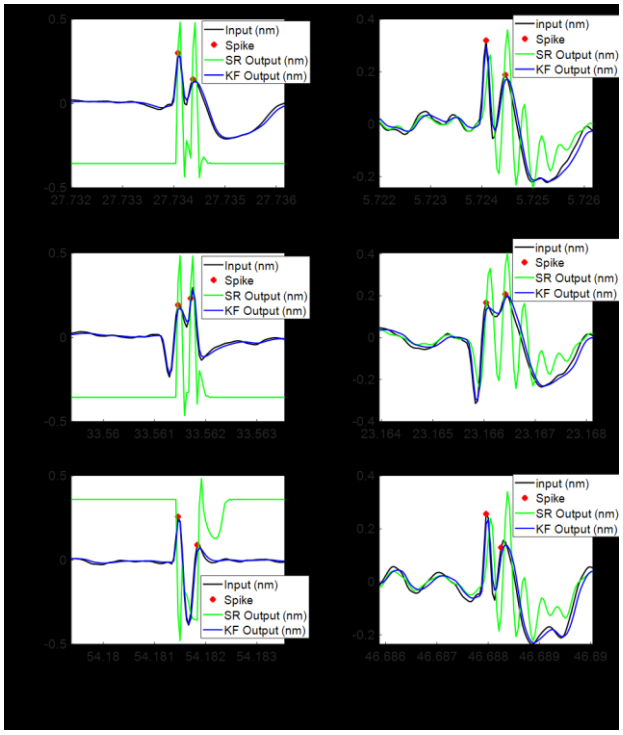

Figure 17. The overlapping spike examples from a low (*Easy1_noise005*) and a high noise (*Easy1_noise02*) recording along with the ShM-UD (SR) and KF outputs. (a) Three overlapping spike examples from the low noise recording. (b) Three overlapping spike examples from high noise recording.

The proposed non-linear SR spike enhancement approach is compared against two linear filtering approaches widely used in spike detection applications. Specifically, the proposed method is compared with a linear state-space model using Kalman filter (KF) [31, 32] and an autoregressive filter (AR) [33, 34, 35] in the frequency domain (Figure 16). This comparison is made in terms of average ΔSNR obtained from ten arbitrarily-selected spikes from a low-noise recording (*Easy1_noise005*) and a high noise recording (*Easy1_noise02*) by integrating the power spectral density over the normal neural spike frequency bandwidth of [300 Hz – 8 kHz]. For the low-noise recording, the SR spike enhancement using ShM-UD achieves an average ΔSNR of 164.9 dB; while Kalman output is 16.6 dB and the AR output is 4.2 dB. For the high-noise recording, the SR model results in 12.9 dB of average ΔSNR; while Kalman and AR filters result in 6.6 dB and -0.7dB, respectively.

Additionally, a time-domain comparison between the SR method and the Kalman filter is made on overlapping spikes. This comparison is limited to Kalman filter, which - unlike the AR filter - produces the filtered spikes in the time-domain. Specifically, a total of six overlapping spike cases from a low noise level recording (*Easy1_noise005*) and a high noise level recording (*Easy1_noise005*) are investigated, three spikes from each (Figure 17). The SR filter approach enables potential detection of overlapping spikes that are as short as

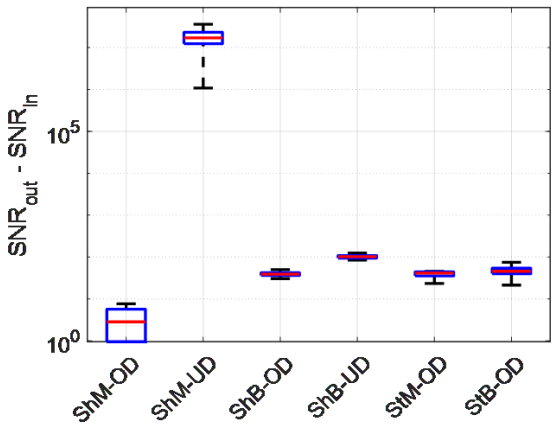

Figure 18. Statistics of SNR improvements of each well-solver configurations with randomly selected well/solver parameters.

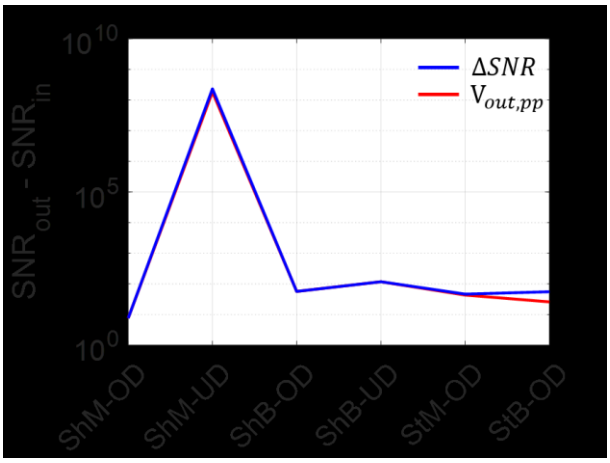

Figure 19. Average $\Delta SNR = SNR_{out} - SNR_{in}$ values calculated using 20 spikes for all configurations. Configurations are optimized for maximizing ΔSNR (blue) and overall peak-to-peak value ($V_{out,pp}$) (red) of the output.

0.1 ms apart for the low-noise recording. For the high-noise recording, detection of overlapping spikes that are apart by 0.25 ms is also potentially possible: Notably, optimization of the system for a high-noise recording leads to a lower damping coefficient than the low-noise recording, which results in a longer ringing period (~ 0.4 ms) that limits the time resolution of the output waveform. However, a careful look into the oscillations reveals that, a spike that follows an initial spike by as short as 0.25 ms increases the amplitude of the oscillations. Accordingly, the output waveform consists of two peaks with similar amplitudes followed by low amplitude oscillations (Figure 17 (b)). On the contrary, Kalman filter output closely follows the input overlapping spike waveform. To compare the spike enhancement performance of overlapping spikes, the range of possible threshold levels that can be used in a successive thresholding stage can be used. For the low-noise recording, average threshold ranges of -0.3 to 0.5 and 0 to 0.4 would identify the two spike events separately for the SR and Kalman filter methods, respectively. For the high-noise recording, average threshold ranges of 0.1 to 0.4 and 0.1 to 0.3 would identify the two spike events separately for the SR and Kalman filter methods, respectively.

The performance of the SR spike enhancement algorithm is directly affected by the model-solver parameter values. To investigate the strength of this dependence between parameter values and ΔSNR, each model is assessed based on the SNR improvement when the parameter values are uniform randomly selected within their respective ranges. A total of 100 ΔSNR calculation is performed for each model configuration for the *Easy1_noise005*. Based on the statistical distribution of the SNR improvement presented in Figure 18, the variances for the models are 7.5 dB, 11 dB, 15 dB, 14 dB, 19 dB, and 14.2 dB for ShM-OD, ShM-UD, ShB-OD, ShB-UD, StM-OD, and StB-OD, respectively. The small variance within each model points that the system is robust inside the parameter range that does not diverge the output.

In this study, where the focus is on SR model performance comparison with respect to spike enhancement, the parametric search is performed based on ΔSNR optimization. A trivial limitation of this approach for parametric optimization in an actual neural monitoring scenario is the necessity for *apriori* knowledge of spike locations in a recording. Although investigation of different metrics for parametric-search-based or other means of parameter optimization is left as a future work; performance of the models optimized based on maximizing another metric, the overall peak-to-peak value of the output ($V_{out,pp}$), is also investigated for the *Easy1_noise005*. In line with the previous results demonstrating the robustness of the system for parameters within the ranges that converge the output, the median ΔSNR obtained from models optimized for maximizing ΔSNR and $V_{out,pp}$ are very close (Figure 19). The difference varies between 3.3 dB for StB-OD and 0 dB for ShB-OD. The model-solver parameters optimized with respect to output SNR and output peak-to-peak are identical, except the $h, a,$ and γ of ShM-UD, and $h, V, R, a,$ and sep of StM-OD and StB-OD.

The striking SNR improvement performance of the ShM-UD comes at the cost of disturbing the original spike waveform shapes, which is critical for spike sorting. To assess if the spikes in a recording can be sorted, a correlation analysis is performed across the spikes from three different neurons in the recordings of the 1st dataset. First a correlation matrix is prepared by calculating the correlations between templates of spike waveforms obtained by ensemble averaging the spikes from different neurons (Table 5). Second, the correlation analysis is repeated on the SR-enhanced output. The correlation is performed between individual output spikes and template spikes obtained by ensemble averaging the output spikes from different neurons (Table 6). Lastly, the difference between the correlations is calculated (Table 7). The Table 7

Table 5. Correlation coefficient values of spikes of the 1st dataset.

		Easy1			Easy2			Difficult1			Difficult2		
		N1	N2	N3	N1	N2	N3	N1	N2	N3	N1	N2	N3
Noise 005	N1	1	0.3175	0.4163	1	0.8071	0.8788	1	0.8007	0.9166	1	0.9739	0.82
	N2	0.3175	1	0.1621	0.8071	1	0.8473	0.8007	1	0.9053	0.9739	1	0.81
	N3	0.4163	0.1621	1	0.8788	0.8473	1	0.9166	0.9053	1	0.82	0.81	1
Noise 01	N1	1	0.3032	0.4069	1	0.8029	0.8752	1	0.8015	0.9212	1	0.9735	0.8235
	N2	0.3032	1	0.163	0.8029	1	0.8399	0.8015	1	0.9039	0.9735	1	0.8107
	N3	0.4069	0.163	1	0.8752	0.8399	1	0.9212	0.9039	1	0.8235	0.8107	1
Noise 015	N1	1	0.3102	0.398	1	0.8033	0.8771	1	0.8061	0.9257	1	0.9722	0.8262
	N2	0.3102	1	0.1669	0.8033	1	0.8494	0.8061	1	0.9093	0.9722	1	0.8082
	N3	0.398	0.1669	1	0.8771	0.8494	1	0.9257	0.9093	1	0.8262	0.8082	1
Noise 02	N1	1	0.3007	0.4197	1	0.8039	0.869	1	0.8005	0.9226	1	0.9747	0.8176
	N2	0.3007	1	0.1452	0.8039	1	0.8353	0.8005	1	0.9017	0.9747	1	0.8102
	N3	0.4197	0.1452	1	0.869	0.8353	1	0.9226	0.9017	1	0.8176	0.8102	1

Table 6. Correlation coefficient values of spikes of the SR-enhanced 1st dataset (Template vs. Individual spikes). Standard deviation values are given in parenthesis.

		Easy1			Easy2			Difficult1			Difficult2		
		N1	N2	N3	N1	N2	N3	N1	N2	N3	N1	N2	N3
Noise005	N1	0.2691 (0.249)	0.279 (0.291)	0.286 (0.052)	-0.012 (0.032)	-0.005 (0.031)	-0.011 (0.028)	0.289 (0.235)	0.339 (0.259)	0.283 (0.282)	0.096 (0.02)	0.142 (0.034)	0.128 (0.032)
	N2	0.2114 (0.095)	0.208 (0.133)	0.165 (0.034)	0.182 (0.018)	0.209 (0.044)	0.192 (0.034)	0.237 (0.057)	0.222 (0.097)	0.244 (0.067)	0.066 (0.016)	0.094 (0.016)	0.076 (0.016)
	N3	0.0302 (0.021)	0.0294 (0.026)	0.024 (0.005)	0.086 (0.01)	0.101 (0.022)	0.088 (0.016)	0.202 (0.135)	0.227 (0.156)	0.199 (0.17)	0.098 (0.03)	0.165 (0.057)	0.155 (0.051)
Noise01	N1	0.8426 (0.134)	0.5138 (0.107)	0.451 (0.051)	0.614 (0.09)	0.689 (0.182)	0.587 (0.128)	0.675 (0.121)	0.767 (0.103)	0.821 (0.094)	0.842 (0.084)	0.832 (0.084)	0.726 (0.081)
	N2	0.2929 (0.107)	0.7394 (0.137)	0.183 (0.067)	0.549 (0.078)	0.643 (0.143)	0.541 (0.107)	0.658 (0.076)	0.813 (0.097)	0.839 (0.069)	0.839 (0.089)	0.876 (0.083)	0.75 (0.081)
	N3	0.4056 (0.15)	0.1622 (0.14)	0.958 (0.059)	0.59 (0.109)	0.673 (0.175)	0.668 (0.124)	0.617 (0.108)	0.776 (0.103)	0.862 (0.083)	0.596 (0.083)	0.634 (0.082)	0.663 (0.065)
Noise015	N1	0.6193 (0.122)	0.3354 (0.123)	0.421 (0.067)	0.654 (0.091)	0.544 (0.121)	0.543 (0.104)	0.661 (0.127)	0.74 (0.105)	0.799 (0.093)	0.867 (0.119)	0.883 (0.096)	0.834 (0.119)
	N2	0.1831 (0.072)	0.7495 (0.205)	0.174 (0.097)	0.604 (0.076)	0.579 (0.125)	0.528 (0.091)	0.63 (0.088)	0.781 (0.096)	0.814 (0.076)	0.853 (0.115)	0.894 (0.088)	0.864 (0.115)
	N3	0.1898 (0.149)	0.1923 (0.255)	0.933 (0.125)	0.625 (0.084)	0.546 (0.137)	0.598 (0.113)	0.599 (0.125)	0.749 (0.115)	0.832 (0.09)	0.83 (0.122)	0.872 (0.097)	0.783 (0.128)
Noise02	N1	0.5719 (0.11)	0.458 (0.115)	0.502 (0.084)	0.7 (0.168)	0.424 (0.087)	0.592 (0.183)	0.634 (0.132)	0.705 (0.118)	0.768 (0.095)	0.769 (0.115)	0.803 (0.112)	0.605 (0.124)
	N2	0.1539 (0.087)	0.6502 (0.08)	0.167 (0.139)	0.716 (0.123)	0.552 (0.069)	0.599 (0.127)	0.61 (0.094)	0.743 (0.102)	0.789 (0.068)	0.744 (0.118)	0.825 (0.115)	0.593 (0.116)
	N3	0.1858 (0.194)	0.1336 (0.147)	0.759 (0.307)	0.674 (0.127)	0.436 (0.096)	0.647 (0.155)	0.576 (0.141)	0.713 (0.134)	0.805 (0.096)	0.603 (0.11)	0.67 (0.123)	0.66 (0.101)

shows that, in majority of the recordings, the dissimilarity between spikes from different neurons increase. On the other hand, the similarity between spikes of a given neuron and the template obtained from all spikes of that neuron decreases significantly (-0.41±0.275), which could potentially decrease the sorting performance. Despite this limitation of the SR spike enhancement using ShM-UD, the spike sorting performance can be potentially improved by feeding the spike sorting stage with the spike waveforms of the input recording, instead of the SR outputs. A similar approach is followed in [4, 36], where the spike enhancement is used for detecting the spike locations in the original recording and the spikes in the original recording are used for sorting. It should be also noted that, in various neural monitoring applications, spike sorting stage is bypassed, and high-level decoding is performed directly on the detected spikes [37, 38, 39, 40]. In such applications, the proposed SR algorithm could be used as the pre-emphasis stage before detection.

One limitation of this study is the use of only GWN in modelling the background noise of an extracellular neural recording. In an actual recording, in addition to GWN, colored noise is also present. Notably, by filtering prior to the SR-based pre-emphasis algorithm, $1/f$ type colored noise can be suppressed. It should be also noted that SR is not limited to GWN. In fact, numerical studies on biological neural network modeling have shown that non-Gaussian noise can enhance the spike coherence [41]. Furthermore, as shown in [42, 43], colored noise can also facilitate SR. Therefore, when using the proposed SR pre-emphasis method, colored noise of the recording could also be potentially facilitated, instead of

Table 7. Correlation coefficient changes with respect to the baseline.

		Easy1			Easy2			Difficult1			Difficult2		
		N1	N2	N3	N1	N2	N3	N1	N2	N3	N1	N2	N3
Noise 005	N1	-0.731	-0.039	-0.13	-1.01	-0.813	-0.89	-0.71	-0.462	-0.633	-0.904	-0.832	-0.692
	N2	-0.106	-0.792	0.003	-0.625	-0.790	-0.655	-0.564	-0.778	-0.662	-0.908	-0.906	-0.734
	N3	-0.386	-0.136	-0.976	-0.792	-0.746	-0.912	-0.715	-0.679	-0.801	-0.722	-0.645	-0.845
Noise 01	N1	-0.157	0.211	0.044	-0.386	-0.114	-0.288	-0.325	-0.035	-0.1	-0.158	-0.141	-0.098
	N2	-0.01	-0.261	0.02	-0.254	-0.357	-0.299	-0.144	-0.187	-0.065	-0.134	-0.124	-0.06
	N3	-0.001	0	-0.042	-0.285	-0.166	-0.332	-0.304	-0.128	-0.138	-0.228	-0.176	-0.337
Noise 015	N1	-0.381	0.025	0.023	-0.346	-0.259	-0.334	-0.339	-0.066	-0.126	-0.134	-0.089	0.008
	N2	-0.127	-0.251	0.007	-0.199	-0.421	-0.322	-0.176	-0.219	-0.096	-0.119	-0.106	0.055
	N3	-0.208	0.025	-0.067	-0.252	-0.303	-0.403	-0.326	-0.16	-0.168	0.004	0.064	-0.217
Noise 02	N1	-0.428	0.157	0.082	-0.3	-0.38	-0.277	-0.366	-0.096	-0.155	-0.231	-0.171	-0.213
	N2	-0.147	-0.35	0.022	-0.087	-0.448	-0.236	-0.19	-0.257	-0.113	-0.23	-0.175	-0.217
	N3	-0.234	0.012	-0.241	-0.195	-0.399	-0.353	-0.347	-0.189	-0.195	-0.216	-0.14	-0.34

filtering it. However, the extent to which the proposed SR method can benefit from colored noise in the recording needs separate investigation, and thus left as a future study.

Another limitation is related to all spikes in the *Easy1_noise005* recording of the first dataset having comparable amplitudes. In an actual recording, neuron-to-neuron variations in channel conductances would lead to spike amplitude variations. Accordingly, two same-amplitude spikes in an actual recording do not necessarily originate from neurons equidistant to the electrode. However, those variations in spike amplitudes do not affect how different well-shape damping-status configurations perform for different SNR_{in}.

It is anticipated that the proposed SR pre-emphasis method could find applications in other spike-like feature detection problems in the general field of neurophysiology. One example is burst suppression feature in electroencephalogram (EEG), which indicates inactivated brain states such as coma and anesthesia [44, 45]. Notably, there are temporal- and frequency- characteristics differences between the bursts in an EEG and spikes in a neural recording. On the other hand, with proper selections of the model and solver parameters, the EEG burst suppression features could potentially be enhanced significantly before detection.

5. Conclusion

In this study, we expand on the initial results of neural spike enhancement facilitating stochastic resonance through interaction of a particle in a monostable well. Our investigation on systems with different well potentials and damping conditions indicate that by changing the number of stable points, wall steepness profile, and damping condition; signal enhancement can be improved. The contribution of additive noise on enhancing a neural spike in such a system can potentially allow detection of spikes originated from far neurons.

References

[1] P. Carlos, J. Martinez, M. J. Ison, R. Quian Quiroga 2012 "How many neurons can we see with current spike sorting algorithms?" *Journal of neuroscience methods* **211** 58-65

[2] D. A. Henze, Z. Borhegyi, J. Csicsvari, A. Mamiya, K.D. Harris, G. Buzsáki 2000 "Intracellular Features Predicted by Extracellular Recordings in the Hippocampus In Vivo," *Journal of Neurophysiology* **84** 390-400

[3] G. Buzsáki 2004 "Large-scale recording of neuronal ensembles," *Nat Neurosci* **7** 446-451

[4] R. Quian Quiroga, Z. Nadasdy, Y. Ben-Shaul 2004 "Unsupervised spike detection and sorting with wavelets and superparamagnetic clustering." *Neural Comput* **16** 1661-1687

[5] H. Semmaoui, J. Drolet, A. Lakhssassi and M. Sawan 2012 "Setting Adaptive Spike Detection Threshold for Smoothed TEO Based on Robust Statistics Theory," *IEEE Transactions on Biomedical Engineering* **59** 474-482

[6] V. Shalchyan, W. Jensen and D. Farina 2012 "Spike Detection and Clustering With Unsupervised Wavelet Optimization in Extracellular Neural Recordings," *IEEE Transactions on Biomedical Engineering* **59** 2576-2585

[7] S. Shahid, J. Walker and L. S. Smith 2010 "A New Spike Detection Algorithm for Extracellular Neural Recordings," *IEEE Transactions on Biomedical Engineering* **57** 853-866

[8] l. Obeid 2007 "Comparison of Spike Detectors based on Simultaneous Intracellular and Extracellular Recordings," *3rd International IEEE/EMBS Conference on Neural Engineering*, *Kohala Coast, HI* 410-413

[9] C.B. Güngör, H. Töreyin 2020 "Facilitating stochastic resonance as a pre-emphasis method for neural spike detection" *J. Neural Eng.* **17** 046047

[10] D. Dai, Q. He 2012 "Multiscale noise tuning stochastic resonance enhances weak signal detection in a circuitry system," *Measurement Science and Technology* **23**

[11] H. Zhang, W. Xiong, S. Zhang, et al. 2016 "Nonstationary weak signal detection based on normalization stochastic resonance with varying parameters," *Sādhanā* **41** 621–632

[12] Z. Zhang, J. Ma. 2019 "Adaptive parameter-tuning stochastic resonance based on SVD and its application in weak IF digital signal enhancement," *EURASIP J. Adv. Signal Process* **24**

[13] J. Liu, Y. Leng, Z. Lai, S. Fan 2018 “Multi-Frequency Signal Detection Based on Frequency Exchange and Re-Scaling Stochastic Resonance and Its Application to Weak Fault Diagnosis,” *Sensors* **18**

[14] S. Lu, Q. He, F, Kong 2015 "Effects of underdamped step-varying second-order stochastic resonance for weak signal detection" *Digital Signal Processing* **36** 93-103

[15] G. Zhang, Y. Yang, T. Zhang 2019 "The characteristic analysis of stochastic resonance and bearing fault diagnosis based on NWSG model driven by trichotomous noise" *Chinese Journal of Physics* **60** 107-121

[16] L. Gammaitoni, P. Hanggi, P. Jung, F. Marchesoni 1998 "Stochastic resonance" *Rev. Mod. Phys.* **70** 223-287

[17] A. S. Asdi, A. H. Tewfik 1995 "Detection of weak signals using adaptive stochastic resonance," *International Conference on Acoustics, Speech, and Signal Processing, Detroit, MI, USA* **2** 1332-1335

[18] C. Duan, Y. Zhan 2016 “The response of a linear monostable system and its application in parameters estimation for PSK signals,” *Physics Letters A* **380** 1358-1362

[19] F. Guo, Y. Zhou, S. Jiang, T. Gu 2006 “Stochastic resonance in a mono-stable system with multiplicative and additive noise,” *Journal of Physics A: Mathematical and General* **39** 13861-13868

[20] Z. Lai, Y. Leng 2016 “Weak-signal detection based on the stochastic resonance of bistable Duffing oscillator and its application in incipient fault diagnosis,” *Mechanical Systems and Signal Processing* **81** 60-74

[21] H. Dong, H. Wang, X. Shen, Z. Jiang 2018 "Effects of Second-Order Matched Stochastic Resonance for Weak Signal Detection," *IEEE Access* **6** 46505-46515 (doi: 10.1109/ACCESS.2018.2866170)

[22] H. Zhang, Q. He, S. Lu, F. Kong 2014 “Stochastic Resonance with a Joint Woods-Saxon and Gaussian Potential for Bearing Fault Diagnosis” *Mathematical Problems in Engineering* **2014** 315901 (doi: 10.1155/2014/315901)

[23] X. Liu, X. Yang, N. Zheng 2012 "Automatic extracellular spike detection with piecewise optimal morphological filter." *Neurocomputing* **79** 132 – 139

[24] F. Franke, R. Quian Quiroga, A. Hierlemann et al. 2015 “Bayes optimal template matching for spike sorting – combining fisher discriminant analysis with optimal filtering.” *J Comput Neurosci* **38** 439–459

[25] H. Xu, Y. Han, X. Han et. al. 2019 “Unsupervised and real-time spike sorting chip for neural signal processing in hippocampal prosthesis.” *Journal of Neuroscience Methods* **311** 111–121

[26] M. Moghaddasi, M. Aliyari Shoorehdeli, Z. Fatahi, A. Haghparast 2020 “Unsupervised automatic online spike sorting using reward-based online clustering.” *Biomedical Signal Processing and Control* **56** 101701

[27] S. Farashi 2018 “Spike detection using a multiresolution entropy based method.” *Biomedical Engineering / Biomedizinische Technik* **63** 361-376 (doi: https://doi.org/10.1515/bmt-2016-0182)

[28] A. Marblestone, B. Zamft, Y. Maguire et al. 2013 “Physical principles for scalable neural recording” *Frontiers in Computational Neuroscience* **7** 137

[29] J. Du, I. H. Riedel-Kruse, J. C. Nawroth et al. 2009 “High-Resolution Three-Dimensional Extracellular Recording of Neuronal Activity With Microfabricated Electrode Arrays” *Journal of Neurophysiology* **101** 1671-1678

[30] J.D. Storey 2003 “The positive false discovery rate: a Bayesian interpretation and the q-value,” *The Annals of Statistics* **31** 2013-2035

[31] A. T. Tzallas, V. P. Oikonomou, D. I. Fotiadis 2006 "Epileptic Spike Detection Using a Kalman Filter Based Approach," *2006 International Conference of the IEEE Engineering in Medicine and Biology Society, New York, NY, USA,* 501-504 doi: 10.1109/IEMBS.2006.260780

[32] V.P. Oikonomou , A.T. Tzallas, D.I. Fotiadis 2007 “A Kalman filter based methodology for EEG spike enhancement,” *Computer Methods and Programs in Biomedicine* **85** 101-108 (doi: 10.1016/j.cmpb.2006.10.003)

[33] H. Chan et al. 2006 "Detection and Characterization of Neural Spikes," *2006 IET 3rd International Conference On Advances in Medical, Signal and Information Processing - MEDSIP 2006, Glasgow, UK* 1-4.

[34] S. E. Paraskevopoulou et. al. 2013 “Feature extraction using first and second derivative extrema (FSDE) for real-time and hardware-efficient spike sorting,” *Journal of Neuroscience Methods* **215** 29-27 (doi: 10.1016/j.jneumeth.2013.01.012)

[35] K. Kajihara et. al. 2018 "Hardware Implementation of Autoregressive Model Estimation Using Burg’s Method for Low-Energy Spectral Analysis," *2018 IEEE International Workshop on Signal Processing Systems (SiPS), Cape Town, South Africa* 199-204 doi: 10.1109/SiPS.2018.8598315

[36] P. K. Wang et. al. 2019 “Low-latency single channel real-time neural spike sorting system based on template matching,” *PLOS ONE* **14** 1-30 (doi: 10.1371/journal.pone.0225138)

[37] H. G. Rey, C. Pedreira, R. Quian Quiroga 2015 “Past, present and future of spike sorting techniques,” *Brain Research Bulletin* **119** 106-117 (doi: 10.1016/j.brainresbull.2015.04.007)

[38] G. W. Fraser et. al. 2009 “Control of a brain-computer interface without spike sorting” *Journal of Neural Engineering* **6** 055004 (doi: 10.1088/1741-2560/6/5/055004)

[39] K. Ganguly, D. Dimitrov, J. Wallis et al. 2011 “Reversible large-scale modification of cortical networks during neuroprosthetic control,” *Nat Neurosci* **14** 662–667 doi: https://doi.org/10.1038/nn.2797

[40] F. Kloosterman, S. P. Layton, Z. Chen, M. A.Wilson 2014 “Bayesian decoding using unsorted spikes in the rat hippocampus” *Journal of Neurophysiology* **111** 217-227 doi: 10.1152/jn.01046.2012

[41] Y. Gong, Y. Hao, Y. Xie, X. Ma, C. Yang 2009 “Non-Gaussian noise optimized spiking activity of Hodgkin–Huxley neurons on random complex networks,” *Biophysical Chemistry* **144** 88-93 (doi: 10.1016/j.bpc.2009.07.001)

[42] P. Hänggi, P. Jung, C. Zerbe et al. 1993 “Can colored noise improve stochastic resonance?,” *J Stat Phys* **70** 25–47 (doi: https://doi.org/10.1007/BF01053952)

[43] D. Nozaki, D. J. Mar, P. Grigg, J. J. Collins 1999 “Effects of Colored Noise on Stochastic Resonance in Sensory Neurons,” *Phys. Rev. Lett.* **82** 2402-2405 (doi: 10.1103/PhysRevLett.82.2402)

[44] S. Ching, P. L. Purdon, S. Vijayan et. al. 2012 “A neurophysiological-metabolic model for burst suppression,”

Proceedings of the National Academy of Sciences **109** 3095-3100 (doi: 10.1073/pnas.1121461109)

[45] Y.Yang, J.T. Lee, J. A. Guidera et. al. 2019 "Developing a personalized closed-loop controller of medically-induced coma in a rodent model," *Journal of Neural Engineering* **16** 036022 (doi: https://doi.org/10.1088/1741-2552/ab0ea4)